UNIVERSITY OF ŽILINA

https://doi.org/10.26552/aer.C.2021.2.4

ANALYSIS OF THE EARTH'S SURFACE INFLUENCE ON THE ACCURACY OF NON DIRECTIONAL BEACON IN MOUNTAIN TERRAIN

Andrej Novák
Air Transport Department
University of Žilina
Univerzitná 8215/1
010 26 Žilina
novak@fpedas.uniza.sk

Alena Novák Sedláčková
Air Transport Department
University of Žilina
Univerzitná 8215/1
010 26 Žilina
sedlackova2@fpedas.uniza.sk

Tomasz Lusiak
Lublin university of Technology,
Poland University
36 Nadbystrzycka,
20-618 Lublin

Anna Stelmach
Warsaw University of
Technology, Faculty of Transport,
ul. Koszykowa 75
00-662 Warsaw

Abstract

This paper deals with the measuring and checking of the Non Directional Beacon using flying laboratory AeroLab 1 at University of Zilina. It is based on the most simple radio navigation concept: a ground-based radio transmitter (the NDB) sends an omnidirectional signal that an aircraft loop antenna receives. Our practical measurement shows that the NDB satisfies ICAO standards and can be used in industrial part of urban area and is functional in spite of the interference. The paper concentrates on the measuring of the Non Directional Beacon (NDB) which is installed close to industrial part of the city. The ADF/NDB navigation system is one of the oldest air navigation system still in use today. One of the paper's goals is to familiarize the aviation public with the practical measurement of this urban area phenomenon in terms of flight safety, which is common in mountainous nations such as Slovakia. The article's other purpose is to educate professionals in the area about this occurrence in terms of its nature as a physical rule, in order to develop solutions to improve the navigation system's measurement accuracy.

Keywords

Measuring, Flight Inspection, NDB, GNSS.

1. Introduction

In aeronautical radio navigation that uses the NDB/ADF system, the main role is played by the radio station - Non-Directional Beacon (NDB). The NDB transmitter has an antenna that transmits a radio signal non-directionally but symmetrically on all sides. The NDB itself does not generate radial aiming information to this navigation point, as is the case with the VOR/DME beacon (Bean & Dutton, n.a.) The pilot's navigation information is the directional bearing angle to the radio station (Bearing). The on-board Automatic Direction Finder generates this bearing information (ADF). It employs the concept of non-directional - circular radiation of the wave front, which is always perpendicular to the radiation source – NDB antenna at any point in the vicinity of the NDB transmitter (Zarihan & Zhang, 2001).

The Non Directional Beacon (NDB) systems provide a navigation capability to suitably equipped aircraft and therefore shall comply with the Standards and Recommended practices (SARPs) in ICAO Annex 10 Volume 1, Chapter 2 (General Provisions for Radio Navigation Aids) and Chapter 3 Section 3.4 (Specification for non-directional radio beacon). A NDB is a low or medium frequency radio beacon that operates in the frequency range 190 to 1,750 kilohertz (kHz). A radio beacon used in conjunction with an Instrument Landing System (ILS) marker is called as Compass Locator (Ahmed & Sharma, 2005).

Under the terms of Act. N. 143/1998 Z. z., 2th April 1998 (Aviation Act) Transport Authority, all civil Medium Frequency (MF) Non-Directional Beacon installations, intended for use in the provision of an Air Traffic Service in the Slovakia, require approval by the Transport Authority. University of Zilina (UNIZA) is able to provide a number of compliant services to assist NDB operators to demonstrate that they meet these SARPs. The following measurements are required to demonstrate compliance with the ICAO SARPs:

- Field Strength.
- Centre Frequency.
- Modulation Depth.
- Morse Ident Transmitted.
- Modulation Frequency.

2. Airborne equipment components for measuring NDB system

The AT-940 Flight Inspection System (FIS) main equipment consists of small and lightweight modules that are easily installed and removed from the aircraft. The airborne modules and related equipment are listed below:

- Host Computer and WinFIS software.
- Avionics Sensor Unit (ASU).
- Signal Processing Unit (SPU).
- Interface cables.
- Optional external avionics sensor(s).

2.1. Required Aircraft Equipment Provisions

In order to operate the AT-940 FIS certain equipment provisions must be installed in the aircraft. The exact provisions required will depend on the system configuration and the end user's specific mission requirements. ATI can prepare an Interface Control Document (ICD) for the end user to ensure the appropriate provisions are specified (Luo & Chen, 2012). The typical required provisions to be installed in the aircraft for operation of the AT-940 are:

- 28 VDC power source for the FIS including appropriate power control switch, circuit
- Breaker, wiring and connectors.
- Dedicated FIS Antennas.
- Attitude and Heading Reference System (AHRS) and Magnetometer.
- Pilot Event switches.
- Interface to aircraft L-Band suppression bus.
- Means of securing the FIS main equipment modules in the aircraft.
- FIS connector interface panel.

2.2. Avionics Sensor Unit (ASU)

The AT-940 ASU contains a Honeywell RNZ-850 Multimode Receiver (MMR) and Garmin G420 TSO GPS receiver with VHF communication. The MMR receives the RF signals and converts them to a format that can be used by the SPU for measurement, display and recording in the WinFIS™ software (Shan & Chen, 1994).

The front panel of the ASU has the MMR cover, under which there is access to the MMR, and the Garmin G420 GPS unit. Please see the manufacturer's operation manuals for information (Thürey et al., 2005; Sukop et al., 2005).

Four volume knobs are also located on the front panel alongside headset jacks and PTT switch. These allow the user to listen to the ident/tones on the individual navigation aids being monitored for NAV, DME, ADF and MKR. The rear panel of the ASU contains six circuit breakers which allow isolation of the individual receivers within the MMR and ASU. The AT-940 GRS contains a DGPS receiver, theodolite interface circuitry, a microprocessor and a telemetry modem. The GRS GPS receiver is positioned over a known point on an airfield, which is entered into the GRS during configuration, and sends DGPS corrections through an RF telemetry link to the SPU in the aircraft. If failure occurs of the DGPS a digital theodolite can be connected and used to track the aircraft (Zhang et al., 2010; Chen et al., 2018).

2.3. Signal Processing Unit (SPU)

Airfield Technology's terminology for the FIS real time computer is Signal Processing Unit (SPU). The SPU does the real-time data acquisition of all flight inspection data. It receives and processes the signals from all the sensors in the FIS. The unit synchronizes and combines the data from the avionics sensors and position reference equipment and transmits it to the host computer (Chen et al., 2018; Ji et al., 2019).

2.4. Position Reference Equipment

Telemetry Receiver. The Telemetry receiver is used to receive Differential Global Positioning System (DGPS) corrections from the Ground Reference Station (GRS). The RS-232 serial data output from the Telemetry receiver is converted to LVTTL prior to being input to the DGPS receivers. The telemetry RS-232 output is input to COM5 on the Serial board for monitoring the status of the telemetry link from the GRS (Jiang et al., 2017).

GPS Antenna Splitter. An active GPS antenna splitter is used to allow all the GPS receivers in the system to share a single antenna on the aircraft. Depending on the specific SPU configuration supplied the GPS splitter may be installed either inside the SPU or externally in the aircraft. Refer to the specific SPU technical manual and/or Interface Control Document for more information (Kazda et al., 2020; Kraus, 2016).

DGPS Receivers. Two independent DGPS receivers are used in the SPU to provide highly accurate and redundant aircraft position data to the system. The receivers receive DGPS corrections from the Ground Reference Station through the Telemetry receiver in the SPU. The RS-232 output from the Telemetry receiver is converted to LVTTL prior to being input to the DGPS receivers. The outputs from the receivers are input to COM6 and COM7 on the Serial board. The pulse-per-second (PPS) signals from the receivers connect to digital inputs on the A/D boards. These are 10 Hz timing signals, which are used by the system as the primary timing reference. Kirschenstein et al., 2018; Myler, 2015).

External AHRS and Magnetometer. The system uses data from the externally mounted AHRS and magnetometer for antenna coordinate transformations (lever arm corrections), antenna pattern compensation and ADF differential bearing error calculation. The AHRS interfaces with the magnetometer through a direct RS-422 connection. Serial RS-232 data from the AHRS is input to the system through COM8 on the Serial board (Sobiech et al., 2017; Ji et al., 2019).

3. Methodology of measuring individual parameters of NDB ZL

Identification check is performed by listening to a Morse code during a circling flight to verify NDB coverage. The identification must be clearly audible. Keying must be accurate and clearly audible throughout the coverage range. The identification must also be correctly coded.

The power drop during identification shall not exceed 0.5 dB and for NDB devices with a required power of 50 NM or more shall not exceed 1.5 dB.

The control of the voice quality is performed during the circling flight. The voice channel must be clearly audible and free of interference throughout the coverage range.

3.1. Rated coverage

Rated coverage, as defined, is a means of determining the actual operation of the NDB in a measurable manner. When checking the rated coverage at its required range, the signal strength

must be at least 70 µV/m. However, this intensity value shall not be exceeded by more than 2 dB. In general, a minimum value of 120 µV/m is sufficient, although this value is not sufficient in areas with very high fault levels. However, it should be noted that the minimum specified field strength values may be insufficient, as they are set only on the basis of a simple comparison of faults in different areas and may be influenced by other factors than will be explained below (Lu et al., 2020; Labun et al., 2020)

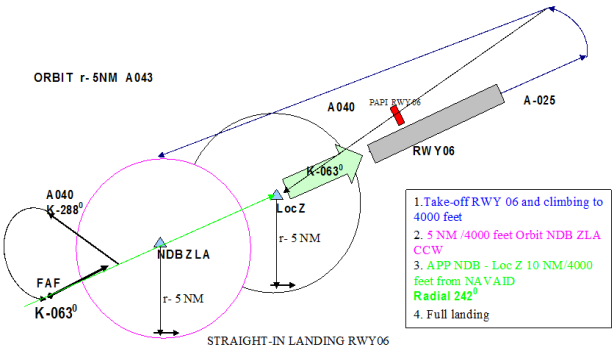

Figure 1: Flight measurement scheme for NDB ZLA, horizontal profile for RWY 06. Source: Authors.

3.2. Effective coverage

Effective coverage is defined as the space surrounding the NDB in which we can obtain real information at a given time. (see Figure 1) When checking the actual coverage, the minimum signal strength is 70 µV/m in the required coverage area. Aiming errors cannot exceed ± 10°. Actual coverage is thus a measure of NDB's performance under normal conditions (Novák et al., 2017).

3.3. Track alignment errors

When checking track alignment errors, the alignment error shall not exceed ±10°. If the alignment errors are of oscillation character, they may exceed this value for less than 8 seconds. When checking approach alignment errors, the alignment error must not exceed ±5°. If the alignment errors are of oscillations nature, they may exceed this value for less than 4 seconds. When checking for alignment errors on hold, the alignment error must not exceed ±5° (Chen et al., 2018; Sobiech et al., 2017).

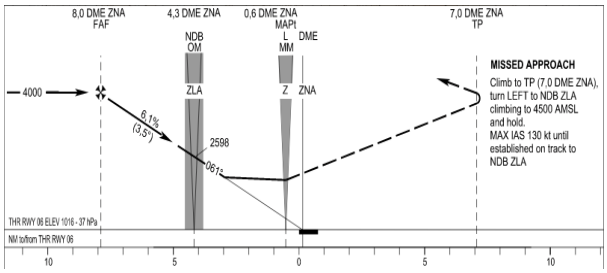

Fig. 2 Flight measurement scheme NDB ZLA, vertical descent profile fo RWY 06. Source: Authors based on Kraus (2016).

4. Practical measuring and testing parameter for ndb zla and NDB ZLA

The ground aid NDB ZLA (identification) is installed in the industrial part of the city Bytča. Installation of test facilities is within the boundaries of the city at the GPS position: LAT: 491210,3N, LON 0183037,6E, and use of the frequency 404 kHz and identification ZLA.

The ground aid NDB Z (identification) is installed in the industrial part of the city Dolný Hričov. Installation of test facilities is within the boundaries of the city at the GPS position: LAT: 491339,4N, LON 0183540,7E, and use of the frequency 508 kHz and identification Z.

4.1. Testing Procedures

1. Take-off from airport Dolný Hričov (LZZI): departure from RWY 06, climb straight ahead via ZLA NDB to 4 000 ft AMSL.
2. At the minimum sector altitude fly two circles (a radius 5 NM, center in NDB ZLA) anti-clockwise (CCW) at an altitude of 4 000 ft. (see Fig. 1)
3. At the minimum sector altitude fly two circles (a radius 5 NM, center in NDB Z) anti-clockwise (CCW) at an altitude of 4 000 ft. (see Fig. 1)
4. Departure within 10 NM from the NDB aid, measurement of back course and checking the aid range identification (Identification marks ZLA). (see Fig. 1)
5. Measurement the NDB approach from FAF (K063) via NDB ZLA and NDB Z full landing runway 06.

4.2. Result from measuring NDB ZLA

The following next four graphs depict dependence of the field strength on the distance or angle. The first phase of flight checking NDB ZLA was the measurement the track in direction ZLA - Z. The measuring flight was conducted at an altitude of 4,000 feet with a gradual descent to an altitude of 4,500 feet. The total length of the measured track was 10 NM including overflying of the NBD ZLA. The voice facility identification test was carried during the flight, identification was clearly identifiable throughout the measured flight path. The measurement sample rate was 10 Hz. The result is in the Fig. 3. The largest recorded facility error was measured in close proximity to the NDB ZLA at a distance 3.37 NM (the error was 13.47°) and was caused by flying over mountains, which are near the NDB ZLA facility.

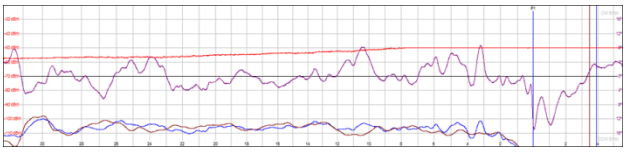

Figure 3: The graphs represent measured values of the first flight segment ZLA – Z. Source: Authors.

The second phase consisted of measurement during the two circuits around the aid at a distance of 5 NM, and of testing the aid. The purpose of the measurement was to check the horizontal cover and facility test in holding. During the test the

checking of aid voice identification was executed, see the result in Fig. 4

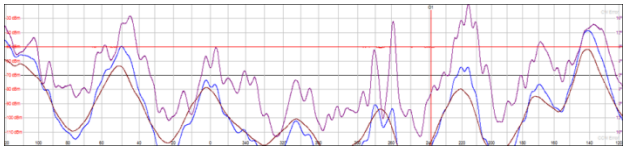

Figure 4: The graphs represented measured values of the second flight segment, orbit 5 NM. Source: Authors.

In the third phase measurement the flight from the facility was using a back course, while the outbound flight was chosen for the existing track between FAF aid and point MAPt. During the testing, the maximum range and reaching of the threshold level of 70 μ/m should be monitored. It is obvious from our measurement that the aid reaches the required minim signal level at the end point of the measurement MAPt , wherein the signal level is -63.5 dBm, that represents 149 mV/m. The measurement result is depicted in the Figure 5.

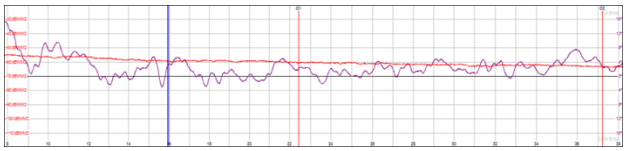

Figure 5: The graphs represent measured values of the third flight segment SLC – PATAC. Source: Authors.

5. Conclusion

Our testing measurement showed that the aid NDB ZLA placed at the test position LAT: 491210,3N, LON 0183037,6E can be used as a navigation aid in Air Navigation Services. It satisfies the requirements of Annex 10, Volume I, for the transmitted power, which cover the device should be at the level of cover 70 μV/m respectively 120 μV/m in areas where there is a big disturbance. Due to the antenna used and the frequency of the device is transmitted power in tolerance according with Annex 10, Volume I, Chapter 3.4. Also, in this case, the electromagnetic wave of the carrier radio navigation NDB signal propagates along the course axis towards the runway 06. If the direction of propagation of the radio wave is along the navigation course axis of the aerodrome, then the wave front of this radio wave is perpendicular to the course axis. The wave front is an imaginary line on which the wave has the same phase and thus the same amplitude. In terms of its principle, the ADF frame antenna shows a direction that is perpendicular to the wave front.

Since the course axis is formed by the NDB signal, this is the direction from which the radio wave is coming, i.e. the direction to the NDB navigation point. If anything affects the tilt of the wave front line, then the ADF will show the wrong direction of NDB alignment. This situation is illustrated on the left side of Fig. 5, where three different positions are marked - the inclinations of the wave front lines (brown) and the indication of the respective direction of the ADF's alignment on the NDB (black arrows). Once the alignment on the NDB is correct - 180º and twice the alignment is with an error of ±5º, i.e. 175º, 185º.

The paper deal with the topic of analyzes the unusual interaction of the electromagnetic waves of the NDB radio navigation signal with the relief of the earth's surface. It analyzes the major impacts, i.e. height changes of the terrain profile and changes in the electrical properties of the surface, which are represented by water surfaces. From the practical use point of view, the reverse targeting of the NDB ZLA is not used, as the NDB Z device is installed on the first kilometer on the approach axis of RWY 06.

Acknowledgment

This work was supported under the project of Operational Programme Integrated Infrastructure: Research and development of contactless methods for obtaining geospatial data for forest monitoring to improve forest management and enhance forest protection, ITMS code 313011V465. The project is co-funding by European Regional Development Fund.

References

Ahmed, M. R, Sharma, S. D. 2005. An investigation on the aerodynamics of a symmetrical airfoil in ground effect Experimental Thermal and Fluid Science, Vol. 29, 2005, pp. 633-647.

Bean, B. R., Dutton, E, n.a. Radio Meteorology, Central Radio Propagation Laboratory, National Bureau of Standards, Boulder, Colorado.

Chen, S., Zhao, H., Huang, C. 2018. Impacts of GNSS radio occultation data on predictions of two super-intense typhoons with WRF hybrid variational-ensemble data assimilation. Journal of Aeronautics, Astronautics and Aviation, 50(4), 347-364. doi:10.6125/JoAAA.201812_50(4).02

Chen, Y., Zhan, X., & Tu, J. 2018. A SVM based GNSS performance assessment with reliable vulnerability degree model. Journal of Aeronautics, Astronautics and Aviation, 50(3), 301-314. doi:10.6125/JoAAA.201809_50(3).07

Ji, K., Zhou, H., & Fan, Y. 2019. GPS vector tracking loop enhancement using a robust cubature kalman filter. Journal of Aeronautics, Astronautics and Aviation, 51(4), 345-354. doi:10.6125/JoAAA.201912_51(4).01

Jiang, C., Chen, S., Chen, Y., Bo, Y., Wang, C., & Tao, W. 2017. Performance analysis of GNSS vector tracking loop based GNSS/CSAC integrated navigation system. Journal of Aeronautics, Astronautics and Aviation, Series A, 49(4), 289-297. doi:10.6125/17-0413-935

Kazda, A., Badanik, B., Tomova, A., Laplace, I., & Lenoir, N. 2013. Future airports development strategies. Komunikacie, 15(2), 19-24.

Kazda, A., Turiak, M., & Gőtz, K. 2020. Airport typology for lcc policy changes: A european perspective. Aviation, 24(3), 90-98. doi:10.3846/aviation.2020.12051

Kirschenstein, M., Ambroziak, R., & Tyburek, P. 2018. Practical use of approach systems for landing at rzeszów-jasionka airport. Paper presented at the Transport

Means - Proceedings of the International Conference, 2018-October 883-888.

Kraus, J. 2016. Determining acceptable level of safety of approach to landing. Paper presented at the Transport Means - Proceedings of the International Conference, , 2016-October 230-235.

Labun, J., Kurdel, P., & Novák, A. 2020. Analysis of the earth's surface influence on the accuracy of ADF. Paper presented at the Transportation Research Procedia, 51 333-341. doi:10.1016/j.trpro.2020.11.036

Lu, N., Zhu, F., Xiao, Y., & Li, X. 2020. The research on EMI of high-speed railway to NDB. IEEE Transactions on Electromagnetic Compatibility, 63(3), 692-701. doi:10.1109/TEMC.2020.3032133

Luo, S. C., Chen, Y.S., Ground effect on flow past a wing with a NACA0015 cross-section. Experimental Thermal and Fluid Science, Vol. 40, 2012, pp. 18-28.

Myler, H. 2015. Design for a source-agile automatic direction finder (ADF). Paper presented at the Proceedings of SPIE - the International Society for Optical Engineering, , 9474 doi:10.1117/12.2176429

Novák, A., Havel, K., & Janovec, M. 2017. Measuring and testing the instrument landing system at the airport zilina. Paper presented at the Transportation Research Procedia, ,28, 117-126. doi:10.1016/j.trpro.2017.12.176

Shan, X., Chen, H. 1994. Simulation of nonideal gases and liquid-gas phase transitions by the lattice Boltzmann equation. Physical Review E, Vol. 49, No. 4, 1994, pp. 2941-2948.

Sobiech, J., Kieliszek, J., Puta, R., Bartczak, D., & Stankiewicz, W. 2017. Occupational exposure to electromagnetic fields in the polish armed forces. International Journal of Occupational Medicine and Environmental Health, 30(4), 565-577. doi:10.13075/ijomeh.1896.00696

Sukop, M., C., 2005. Thorne JTD, Lattice Boltzmann Modeling. Germany: Springer-Verlag, 2005.

Thürey, N., Rüde, U., Körner, C. 2005. Interactive Free Surface Fluids with the Lattice Boltzmann Method, Technical Report 05-4, University of Erlangen-Nuremberg, Germany 2005.

Zerihan, J., Zhang, X. 2001. Aerodynamics of gurney flaps on a wing in ground effect. AIAA Journal, Vol. 39, No. 5, 2001, pp. 772-780.

Zhang, R. L., Di, Q. F., Wang, X. L., Gu, C.Y. 2010, Numerical study of wall wettabilities and topography on drag reduction effect in micro-channel flow by Lattice Boltzmann Method, Journal of Hydrodynamics, Ser. B, Vol. 22, No. 3, 2010, pp. 366-372.